Available online at www.sciencedirect.com
SCIENCE DIRECT®
International Journal of Heat and Mass Transfer 49 (2006) 2939–2949
International Journal of HEAT and MASS TRANSFER
www.elsevier.com/locate/ijhmt

One-dimensional mixed MHD convection

Giuseppe Sposito, Michele Ciofalo *

Dipartimento di Ingegneria Nucleare, Università di Palermo, Viale delle Scienze, I-90128 Palermo, Italy

Received 3 August 2004
Available online 24 April 2006

Abstract

The parallel, fully developed flow of an electrically conducting fluid between plane parallel walls under the simultaneous influence of a driving pressure head, buoyancy, and magnetohydrodynamic (MHD) forces is studied. The fluid is assumed to be internally heated and the flow is modeled as one-dimensional and incompressible, while the Boussinesq approximation is adopted for the buoyancy terms. Analytical solutions are obtained for temperature, velocity and electrical potential under different electrical boundary conditions, forced to natural convection intensity ratios and values of the magnetic induction. Generalized working charts are presented which synthetically describe the system's operation as an EM pump, a MHD generator, a thermal engine or a pure dissipator.

1. Introduction

Magnetohydrodynamics (MHD) deals with the motion of electrically conducting fluids under the influence of a magnetic field. The birthdate of MHD may be identified with the first experiments by Faraday who attempted to measure the electric potential induced between the opposite banks of the Thames river by the motion of the (weakly) conducting water in the Earth's magnetic field [8]. The principle behind Faraday's (unsuccessful) experiment is the same which underlies modern MHD flow meters. About in the same period, Ritchie developed a rudimentary electromagnetic pumping device, although the first working MHD pump was presented only much later [13].

Currently, MHD effects are widely exploited in different industrial processes ranging from metallurgy to the production of pure crystals [12]. A field in which MHD will play an essential role is nuclear fusion, where it is involved in at least two different problems: the confinement and dynamics of plasma, and the behaviour of the liquid metal alloys employed in some of the currently considered designs of tritium breeding blankets.

Consider the duct in Fig. 1, in which a conducting fluid flows upward with velocity $\mathbf{w}$ in the presence of a horizontal magnetic induction field $\mathbf{B}$. The Lorentz force $\mathbf{F} = Q\mathbf{w} \times \mathbf{B}$ acting on electric charges Q convected by the fluid gives rise to an induced current density $\mathbf{j}_i = \sigma\mathbf{w} \times \mathbf{B}$, σ being the fluid's electric conductivity. At the same time, charge separation creates through the duct a distribution of electric potential φ; this results in a diffusive electric current of density $\mathbf{j}_d = -\sigma\nabla\varphi$, opposite to $\mathbf{j}_i$. The overall current density $\mathbf{j} = \sigma(\mathbf{w} \times \mathbf{B} - \nabla\varphi)$ is shown in Fig. 1 as possessing the same direction of $\mathbf{j}_i$, but this is not necessarily true. The interaction between the current density $\mathbf{j}$ and the magnetic induction field $\mathbf{B}$ causes in its turn a magnetohydrodynamic force of volume density $\mathbf{f} = \mathbf{j} \times \mathbf{B}$; this may locally oppose or aid the fluid's motion according to whether the induced or the diffusive current (i.e., $\mathbf{j}_i$ or $\mathbf{j}_d$) prevails.

Fig. 2(a) reports a cross-section of the duct. The fluid's velocity $\mathbf{w}$ is orthogonal to the section and directed upward, and the arrows indicate, in a schematic way, the direction of the total current density in the different regions of the section. The walls lying orthogonal to $\mathbf{B}$ are called *Hartmann walls*, while those lying parallel to $\mathbf{B}$ are called *side walls*. A typical velocity profile along the line $a - a$ parallel to $\mathbf{B}$ is reported in Fig. 2(b). In the central region of the duct, where the maximum speed is attained, the

* Corresponding author. Tel.: +39 091 232 225; fax: +39 091 232 215.
E-mail address: ciofalo@din.din.unipa.it (M. Ciofalo).

0017-9310/$ - see front matter © 2006 Elsevier Ltd. All rights reserved.
doi:10.1016/j.ijheatmasstransfer.2006.02.035

Nomenclature

B, B	magnetic induction (T)
D	distance between parallel walls (m)
F, F	Lorentz force (N)
f, f	Lorentz force per unit volume (N m^{-3})
g, g	acceleration due to gravity (m s^{-2})
Gr	Grashof number
j, j	electric current density (A m^{-2})
J	dimensionless electric current density
L	dimensionless extrapolation distance
M	Hartmann number
N_p	pressure head number
p	pressure (N m^{-2})
P	dimensionless power
Q	electric charge (C)
q	volumetric power density (W m^{-3})
t	temperature (K)
T	dimensionless temperature
V	electric potential difference (V)
w, w	velocity (m s^{-1})
W	dimensionless velocity
x, y, z	Cartesian co-ordinates (m)
X	dimensionless length

Greek symbols

β	thermal expansion coefficient (K^{-1})
λ	thermal conductivity (W m^{-1} K^{-1})
μ	viscosity (N s m^{-2})
ν	kinematic viscosity (m^2 s^{-1})
ρ	density (kg m^{-3})
σ	electric conductivity (Ω^{-1} m^{-1})
φ	electric potential (V)
Φ	dimensionless electric potential

Subscripts and averages

CL	centerline
d	diffusive
E	electrical
i	induced
M	mechanical
x, y, z	Cartesian components
$\bar{\Psi}$	average value of generic quantity Ψ

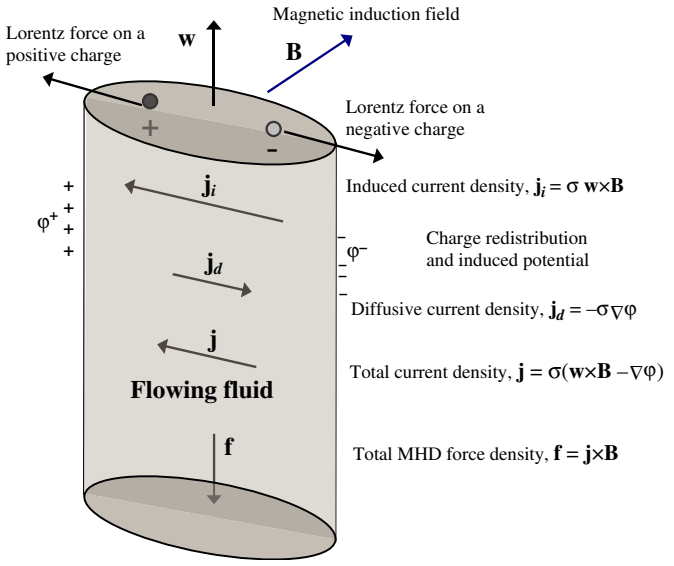

Fig. 1. Lorentz forces and electric currents as an electrically conducting fluid flows upward in a straight duct with velocity **w** in the presence of a horizontal magnetic induction field **B**.

electromagnetic forces oppose the fluid's motion; this *magnetic braking* causes a flattened velocity profile. Near the Hartmann walls, since the fluid's speed necessarily vanishes because of the no slip conditions, the diffusive current prevails and the resulting electromagnetic forces aid the fluid's motion, giving rise to a steep velocity profile in thin boundary layers (*Hartmann layers*). Similar, but thicker, boundary layers are formed on the side walls.

Current lines are represented in Fig. 3 for different electric conductivities of the solid walls. The intensity of the total currents in the fluid (hence, of the total MHD forces) depends on the overall resistance encountered by the current loops, which in turn includes the tiny bulk flow resistance and the return resistance associated to the Hartmann layers and to the solid walls, the last two arranged in parallel. In the case of highly conducting walls, current loops close themselves entirely in the walls, the return resistance becomes negligible and the only loop electric resistance is the bulk resistance of the liquid metal; as a consequence, MHD forces oppose the fluid's motion everywhere, overall currents and braking MHD forces are highest, and the largest MHD damping of the flow is obtained. In the opposite case of electrically insulating walls, current loops close themselves only through the thin Hartmann layers; the loop electric resistance is highest, while currents are small and so are MHD braking effects. An intermediate behaviour is obtained for finite conductivity walls.

The above remarks make it clear, although on a purely qualitative basis, that many MHD effects on the flow of an electrically conducting fluid depend on the way current loops establish themselves in the domain of interest; as such, they require at least two spatial dimensions in addition to the direction of the fluid's velocity **w**. In fact, a large number of published computational studies on MHD flows have been conducted in two dimensions and have assumed conditions of fully developed flow or channels of infinite

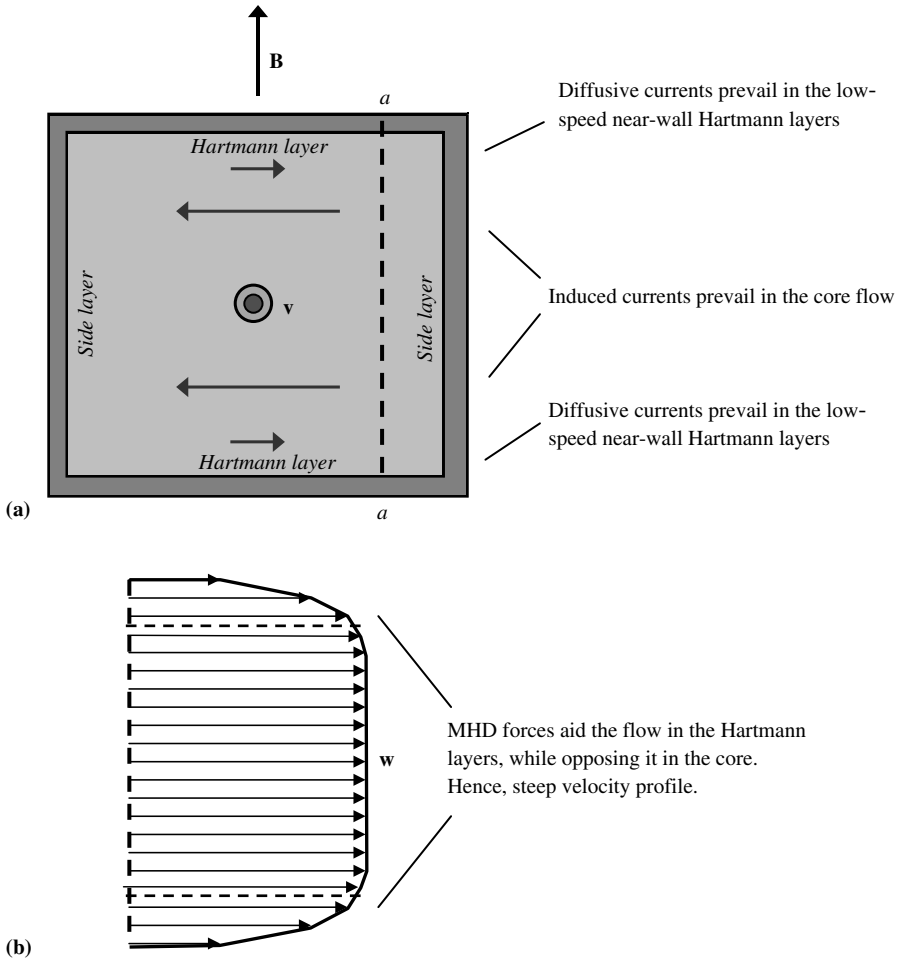

Fig. 2. Current and flow distribution in a cross-section of a straight duct. Top: current densities; bottom: velocity profile along a line *a–a* parallel to **B**.

length to dispose of the third dimension, see for example Bühler [1], Di Piazza and Bühler [4], Ciofalo and Cricchio [2]. A few papers have dealt with fully three-dimensional MHD problems, see for example Tagawa and Ozoe [17], Di Piazza and Ciofalo [6,7], Ciofalo and Cricchio [3].

However, two- or three-dimensional MHD problems are rarely amenable to exact (analytical) solutions, and a combination of asymptotic analysis and of numerical methods usually have to be employed, which often obscures the meaning of the results as closed form expressions for various quantities of physical relevance cannot be written.

On the other hand, exact solutions are possible if one restricts the attention to one-dimensional MHD problems such as that schematically shown in Fig. 4. Here, an electrically conducting fluid flows along z in a vertical channel delimited by infinite plane parallel walls orthogonal to x and placed at a distance D, under the influence of an externally imposed driving pressure gradient and of the MHD forces caused by the interaction of the flow with a uniform magnetic induction field **B**, directed along y. Buoyancy forces, caused by internal power generation of volume density q and/or by differential heating of the two walls, can easily be included thus giving rise to mixed MHD convection, a condition which has been very little studied in the literature so far [11,15,16]. No slip conditions can be assumed at the walls, although more general conditions, such as those of differentially sliding walls, could easily be taken into account.

2. Governing equations

For steady-state conditions, one-directional, parallel, fully developed MHD flow, the problem in Fig. 4 is governed by the set of one-dimensional equations discussed here below.

First, by assuming constant physical properties and using the Boussinesq approximation for buoyancy, the vertical momentum (MHD Navier–Stokes) equation can be written:

$$-\frac{\mathrm{d}p}{\mathrm{d}z}+\mu\frac{\mathrm{d}^2w}{\mathrm{d}x^2}+g\beta\rho(t-\bar{t})-j_xB=0 \tag{1}$$

in which j_x is the only nonzero component of the current density vector **j**. As discussed in Section 1, it can be expressed as the algebraic sum of an *induced* and a *diffusive* contribution:

$$j_x=-\sigma wB-\sigma\frac{\mathrm{d}\varphi}{\mathrm{d}x} \tag{2}$$

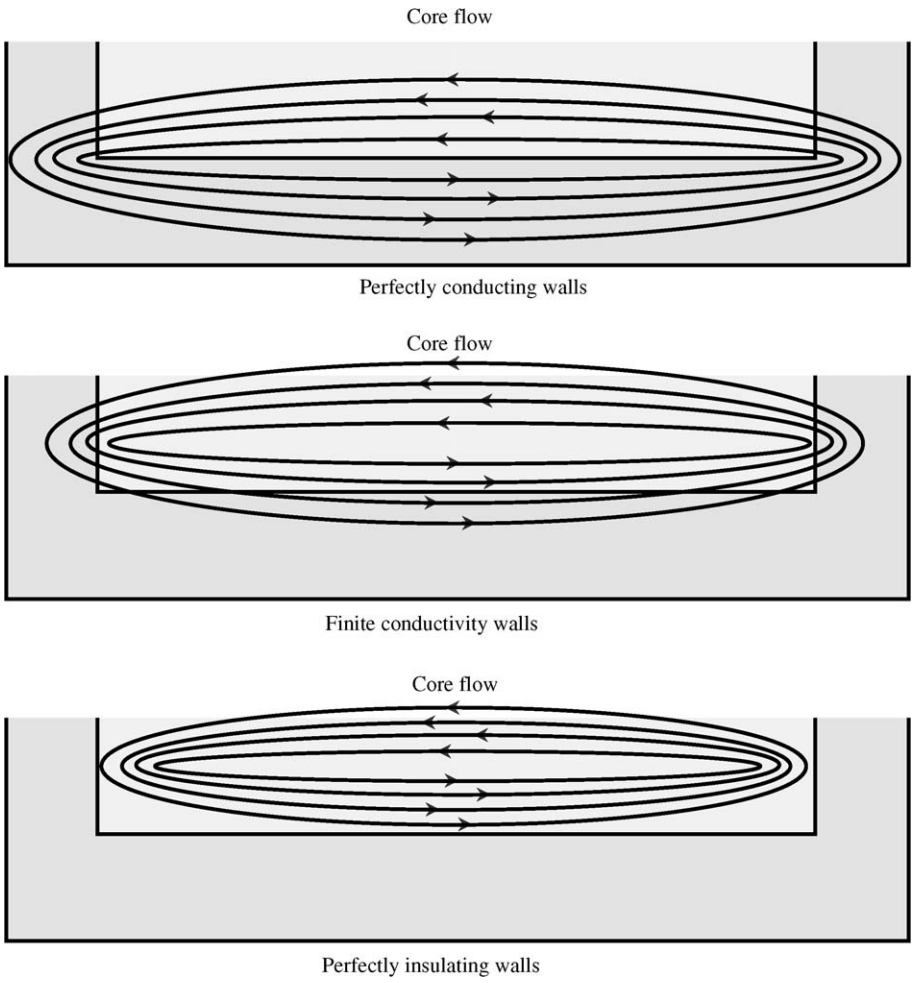

Fig. 3. Schematic representation of current lines for different conductivities of the walls.

By substituting Eq. (2) for j_x into Eq. (1), one has the following modified Helmholtz equation for the vertical velocity w:

$$\mu\frac{\mathrm{d}^2w}{\mathrm{d}x^2}-\sigma B^2w=\frac{\mathrm{d}p}{\mathrm{d}z}-g\beta\rho(t-\bar{t})+\sigma B\frac{\mathrm{d}\varphi}{\mathrm{d}x} \tag{3}$$

Second, the Poisson equation for the electrical potential reduces to:

$$\frac{\mathrm{d}^2\varphi}{\mathrm{d}x^2}=-B\frac{\mathrm{d}w}{\mathrm{d}x} \tag{4}$$

Finally, the heat transport equation reduces to the conduction equation:

$$\frac{\mathrm{d}^2t}{\mathrm{d}x^2}=-\frac{q}{\lambda} \tag{5}$$

in which λ is the thermal conductivity of the fluid. Eqs. (3)–(5) are coupled in such a way that only the heat Eq. (5) can be independently solved for the temperature t, whereas the electric potential φ depends on the w velocity and this latter depends both on φ and on the temperature t.

The above equations can be made dimensionless by using for the various physical quantities the scales summarized in Table 1.

Note that the viscous scale ν/D was used here for the velocity w, but several alternatives would be possible, including magnetohydrodynamic, buoyant, and diffusive scales. The present choice offers the advantage that the scale ν/D can never vanish for real fluids.

By using the above scales and defining the following dimensionless groups:

$$\text{Pressure head number}\quad N_p=-\frac{\mathrm{d}p}{\mathrm{d}z}\frac{\rho D^3}{\mu^2} \tag{6}$$

$$\text{Grashof number}\quad Gr=\frac{g\beta qD^5}{\lambda\nu^2} \tag{7}$$

$$\text{Hartmann number}\quad M=BD\sqrt{\frac{\sigma}{\mu}} \tag{8}$$

Eqs. (3)–(5) can be re-written as:

$$\frac{\mathrm{d}^2W}{\mathrm{d}X^2}-M^2W=-\frac{Gr}{8}(T-\bar{T})+M^2\frac{\mathrm{d}\Phi}{\mathrm{d}X}-N_p \tag{9}$$

$$\frac{\mathrm{d}^2\Phi}{\mathrm{d}X^2}=-\frac{\mathrm{d}W}{\mathrm{d}X} \tag{10}$$

$$\frac{\mathrm{d}^2T}{\mathrm{d}X^2}=-8 \tag{11}$$

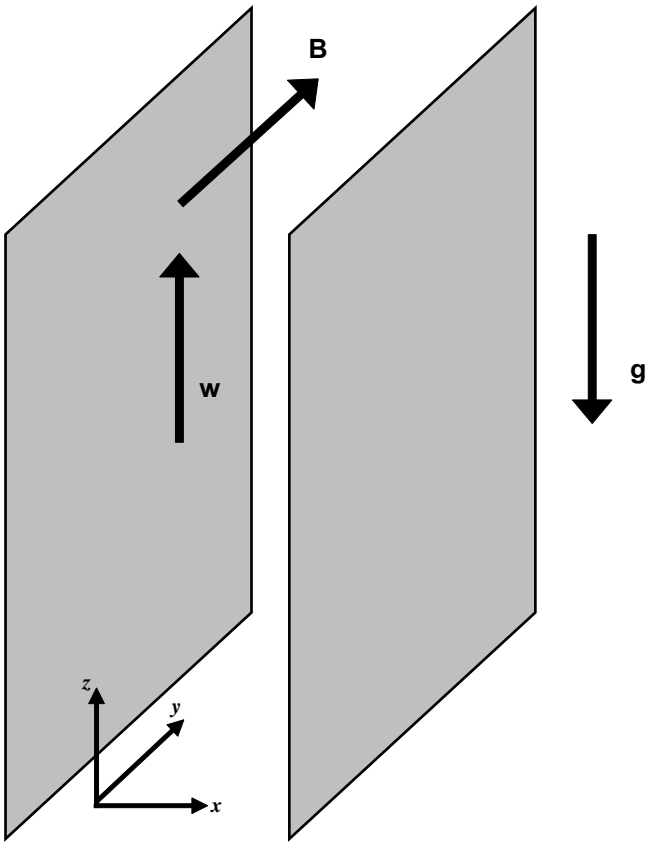

Fig. 4. Geometry studied in the present work (channel delimited by infinite plane parallel walls).

Table 1
Normalization scales

Physical quantity	Dimensioned variable	Scale used	Dimensionless variable
Length	x (m)	D	$X = \frac{x}{D}$
Velocity	w (m s^{-1})	$\frac{\nu}{D}$	$W = \frac{wD}{\nu}$
Temperature	t (K)	$\frac{qD^2}{8\lambda}$	$T = (t - t_w)\frac{8\lambda}{qD^2}$
Electric potential	φ (V)	νB	$\Phi = \frac{\varphi}{\nu B}$
Electric current density	j (A m^{-2})	$\frac{\nu B\sigma}{D}$	$J = \frac{jD}{\nu B\sigma}$

while the electric current density in Eq. (2) is replaced by its dimensionless counterpart:

$$J_x = -\left(W + \frac{\mathrm{d}\Phi}{\mathrm{d}X}\right) \tag{12}$$

3. Solutions for equi-potential walls

Among all possible boundary conditions, consider first those of no slip on still walls for the vertical velocity; isothermal walls at $t = t_w$ for the temperature; and equi-potential (infinitely electrically conducting) walls at $\varphi = 0$ for the electric potential. In dimensionless terms, these are expressed by:

$$W\left(\pm\frac{1}{2}\right) = 0 \tag{13}$$

$$\Phi\left(\pm\frac{1}{2}\right) = 0 \tag{14}$$

$$T\left(\pm\frac{1}{2}\right) = 0 \tag{15}$$

The heat Eq. (11) with BCs (15) immediately yields the parabolic temperature distribution:

$$T(X) = 1 - 4X^2 \tag{16}$$

whose mean value is:

$$\overline{T} = \frac{2}{3} \tag{17}$$

The electric potential Eq. (10) can be formally integrated once to give:

$$\frac{\mathrm{d}\Phi}{\mathrm{d}X} = -W + C_1 \tag{18}$$

in which C_1 is an integration constant to be determined later by imposing the boundary conditions on Φ. Taking Eqs. (16)–(18) into account, the momentum Eq. (9) becomes:

$$\frac{\mathrm{d}^2 W}{\mathrm{d}X^2} = -\frac{Gr}{8}\left(\frac{1}{3} - 4X^2\right) + M^2 C_1 - N_p \tag{19}$$

By integrating this twice with respect to X, and imposing the boundary conditions (13), one has:

$$W(X) = \frac{Gr}{384} + \frac{N_p}{8} - \frac{C_1 M^2}{8} + \frac{1}{2}\left(-\frac{Gr}{24} + C_1 M^2 - N_p\right)X^2 + \frac{Gr}{24}X^4 \tag{20}$$

This last expression, which still depends upon the integration constant C_1, can be substituted for W in Eq. (18), which, once integrated again, gives:

$$\Phi(X) = \left[C_1\left(1 + \frac{M^2}{8}\right) - \frac{Gr}{384} - \frac{N_p}{8}\right]X - \frac{1}{6}\left(C_1 M^2 - N_p - \frac{Gr}{24}\right)X^3 - \frac{Gr}{120}X^5 + C_4 \tag{21}$$

Finally, by imposing the boundary conditions (14) one obtains the two constants C_1 and C_4 which, once substituted in Eqs. (20) and (21), yield the explicit profiles of W and Φ as functions of X:

$$W(X) = \frac{1}{8}\left(\frac{Gr}{48} + N_p - \frac{M^2}{M^2 + 12}\frac{60N_p + Gr}{60}\right) + \frac{1}{2}\left(\frac{M^2}{M^2 + 12}\frac{60N_p + Gr}{60} - \frac{Gr}{24} - N_p\right)X^2 + \frac{Gr}{24}X^4 \tag{22}$$

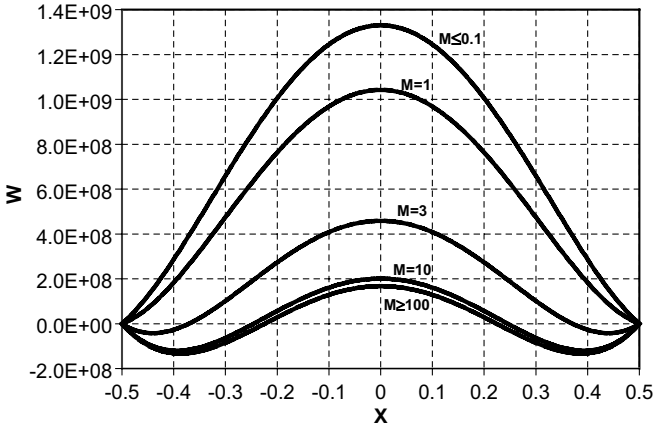

Fig. 5. Dimensionless velocity for $Gr = 10^{10}$, $N_p = 10^9$ and different values of M (equi-potential walls).

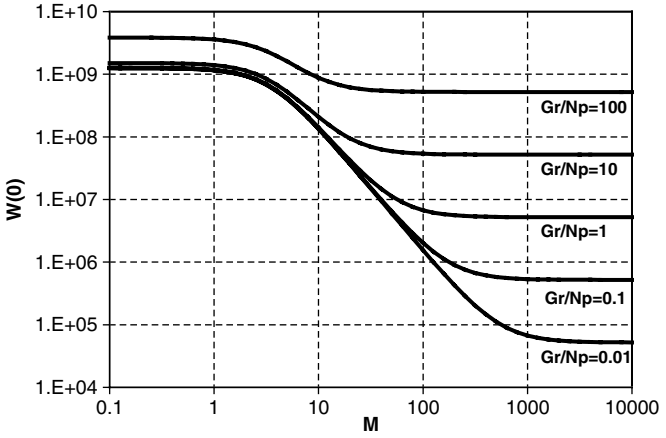

Fig. 7. Dimensionless centerline velocity as a function of the Hartmann number M for $N_p = 10^{10}$ and different values of the Gr/N_p ratio.

$$\Phi(X) = \frac{1}{96}\left(\frac{60N_p + Gr}{5}\frac{M^2+8}{M^2+12} - \frac{48N_p + Gr}{4}\right)X + \frac{1}{72}\left(-\frac{60N_p + Gr}{5}\frac{M^2}{M^2+12} + \frac{24N_p + Gr}{2}\right)X^3 - \frac{Gr}{120}X^5 \tag{23}$$

Profiles of W and Φ are reported in Figs. 5 and 6 for an arbitrary choice of the Grashof and pressure head numbers ($Gr = 10^{10}$, $N_p = 10^9$) and different values of the Hartmann number M. The centerline velocity $W_{CL} = W(0)$ tends to the following limiting values for $M = 0$ and $M \to \infty$, respectively:

$$W_{CL}(M = 0) = \frac{Gr}{384} + \frac{N_p}{8} \tag{24a}$$

$$W_{CL}(M \to \infty) = \frac{Gr}{1920} \tag{24b}$$

Therefore, as the magnetic induction increases, the forced-flow velocity component is completely suppressed, but the velocity component associated with natural convection can only be reduced by a factor of 5 at most. This is also illustrated in Fig. 7, which reports the dimensionless centerline velocity W_{CL} as a function of the Hartmann number M for $N_p = 10^{10}$ and different values of the Gr/N_p ratio. The figure also shows that MHD effects become significant as soon as the Hartmann number exceeds the value of ~1. Note that this behaviour is at variance with that observed in *two-dimensional* channel flow, where MHD effects become significant only for M greater than ~100 and where also the natural convection component of the velocity is completely suppressed by large values of the magnetic induction [3].

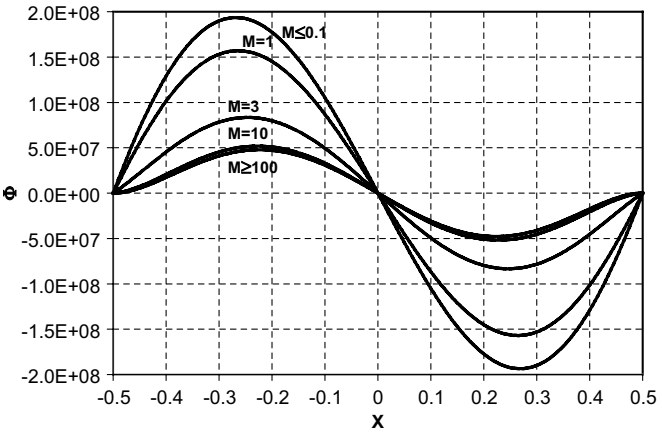

Fig. 6. Dimensionless potential for $Gr = 10^{10}$, $N_p = 10^9$ and different values of M (equi-potential walls).

The average W velocity is:

$$\overline{W} = \frac{1}{M^2+12}\frac{60N_p + Gr}{60} \tag{25}$$

while, by substituting Eq. (18) for $d\Phi/dX$ into Eq. (12), one obtains for the current density J_x the constant value:

$$J_x = -\frac{1}{M^2+12}\frac{60N_p + Gr}{60} \tag{26}$$

Therefore, in the present dimensionless form, one has $J_x = -\overline{W}$ (constant). However, the behaviour of mean velocity and electric current as functions of the Hartmann number is best appreciated by considering these quantities in dimensioned, rather than dimensionless, form. This is shown in Fig. 8 which reports $\bar{w}$ and j_x for a particular choice of the geometrical dimension D of the channel and of the physical properties of the fluid (corresponding to the eutectic 83%Pb–17%Li alloy). It can be observed that the electric current attains its maximum values for $M \approx 3$, which is close to the limiting value of ~1 above which a significant reduction of the mean velocity is observed. The difference with respect to *two-dimensional* channel flow [3], in which current maxima are attained at $M \approx 100$, is again clear. The difference can be explained by the fact that in two-dimensional flows, as discussed in Section 1, the electric currents induced by MHD effects close themselves through the Hartmann layers and/or the solid walls, whose electric resistance limits the current intensity and makes high values

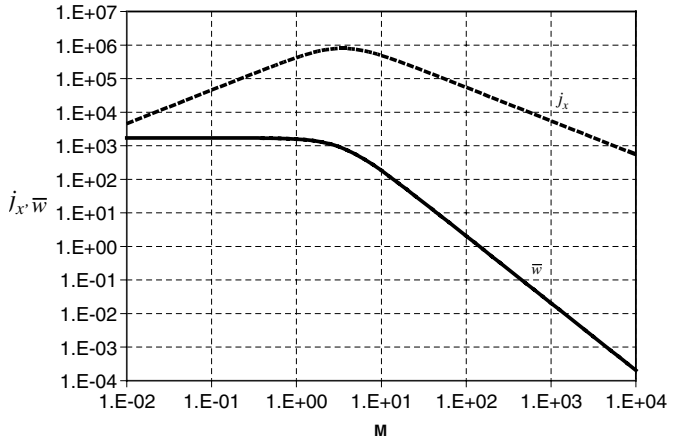

Fig. 8. Dimensioned mean velocity and electric current as functions of the Hartmann number M for Pb–17Li, D=0.15, $N_p = 10^{10}$, $Gr = 10^{11}$ ($Gr/N_p = 10$).

of the magnetic induction (Hartmann numbers) necessary for significant damping effects to occur. On the contrary, in the present one-dimensional model no return resistance is encountered by the electric current, which makes lower values of the Hartmann number sufficient to cause significant MHD braking effects.

Eqs. (25) and (26) show that both the average velocity and the current density vanish for:

$$N_p = -\frac{Gr}{60} \tag{27}$$

If the above condition is satisfied, Eqs. (25) and (26) show that one has $\bar{W} = 0$, $J_x = 0$, i.e., both the net flow rate and the electric current vanish, hence there are no MHD effects on the flow no matter how large the Hartmann number M. Eq. (22) then gives for $W(X)$ the following profile, which is independent of M and thus of the applied magnetic induction B_x:

$$W = \frac{Gr}{1920}(1 - 24X^2 + 80X^4) \tag{28}$$

This coincides with the W profile obtained for internal heating in the absence of MHD effects by Geršuni and Žukovitskij [9] (as reported, e.g., by Kulacki and Richards [10]), and later by Di Piazza and Ciofalo [5].

4. Solutions for an imposed potential difference between opposite walls

The above solutions can easily be generalized to the case in which a difference of electric potential V (made dimensionless by the same scale used for φ) is imposed between the opposite walls of the channel. The boundary condition (14) is replaced by:

$$\Phi\left(-\frac{1}{2}\right) = +\frac{V}{2}; \quad \Phi\left(+\frac{1}{2}\right) = -\frac{V}{2} \tag{29}$$

Note that the pressure head number N_p and the potential difference V are taken to be positive if they tend to drive the fluid towards positive z and the electric current towards positive x.

Accordingly, the solutions obtained above for W, Φ and J_x are replaced by:

$$W(X) = \frac{1}{8}\left(\frac{Gr}{48} + N_p - \frac{M^2}{M^2+12}\frac{60N_p + Gr - 720V}{60}\right) + \frac{1}{2}\left(\frac{M^2}{M^2+12}\frac{60N_p + Gr - 720V}{60} - \frac{Gr}{24} - N_p\right)X^2 + \frac{Gr}{24}X^4 \tag{30}$$

$$\Phi(X) = \frac{1}{96}\left(\frac{60N_p + Gr - 720V}{5}\frac{M^2+8}{M^2+12} - \frac{48N_p + Gr}{4}\right)X + \frac{1}{72}\left(-\frac{60N_p + Gr - 720V}{5}\frac{M^2}{M^2+12} + \frac{24N_p + Gr}{2}\right)X^3 - \frac{Gr}{120}X^5 \tag{31}$$

$$J_x = -\frac{1}{M^2+12}\frac{60N_p + Gr - 720V}{60} \tag{32}$$

while the average velocity expressed by Eq. 24 becomes now:

$$\overline{W} = \frac{1}{M^2+12}\frac{60N_p + Gr + 60M^2V}{60} \tag{33}$$

4.1. Working charts for the case of no buoyancy

Consider first the simple case in which no buoyancy forces act on the fluid. By letting $Gr = 0$ in Eqs. (32) and (33) one has:

$$J_x = -\frac{(N_p - 12V)}{M^2+12} \tag{34}$$

$$\overline{W} = \frac{N_p + M^2V}{M^2+12} \tag{35}$$

By analogy with the working diagram of a hydraulic pump, working charts for the present generalized MHD engine can be drawn in a plane having abscissa $\overline{W}$ (directly proportional to the volumetric flow rate) and ordinate N_p (pressure head number, corresponding to the prevalence of a centrifugal pump).

By solving Eq. (35) for V and substituting in Eq. (34), one has:

$$J_x = \frac{12\overline{W} - N_p}{M^2} \tag{36}$$

The mechanical power provided by the system (positive if the average velocity is opposite to the external applied force) can be immediately expressed as:

$$P_M = -N_p\overline{W} \tag{37}$$

The electric power provided by the system is $-VJ_x$ and is positive if the electric current is opposite to the imposed electric potential gradient. By using Eq. (36) for J_x and solving Eq. (35) for V one has:

$$P_E = -VJ_x = -\frac{1}{M^4}[N_p^2 - (M^2+24)N_p\overline{W} + 12(M^2+12)\overline{W}^2] \tag{38}$$

Therefore, one has $P_M = 0$ if $\overline{W} = 0$ (N_p axis) or $N_p = 0$ ($\overline{W}$ axis), while $P_E = 0$ if $N_p = 12\overline{W}$ or $N_p = (M^2 + 12)\overline{W}$ (two straight lines crossing the first and third quadrants). It is thus possible to build eight-region working charts of the kind shown in Fig. 9 for two values of the Hartmann number M. In these charts constant-P_E and constant-P_M lines are reported, and the regions of the $\overline{W} - N_p$ plane where $P_E > 0$ and $P_M > 0$ are highlighted.

The comparison of the two graphs (a) and (b) in Fig. 9 shows that the amplitude of the two sectors representing the MHD generator mode ($P_E > 0$) increases as M (i.e., the imposed magnetic induction field) increases, whereas the two sectors representing the MHD pump mode ($P_M > 0$) have a fixed amplitude of 90°, independent of the value of M. In the four remaining regions the system works as a pure dissipator since it absorbs both electric and mechanical power ($P_E \leqslant 0$, $P_M \leqslant 0$).

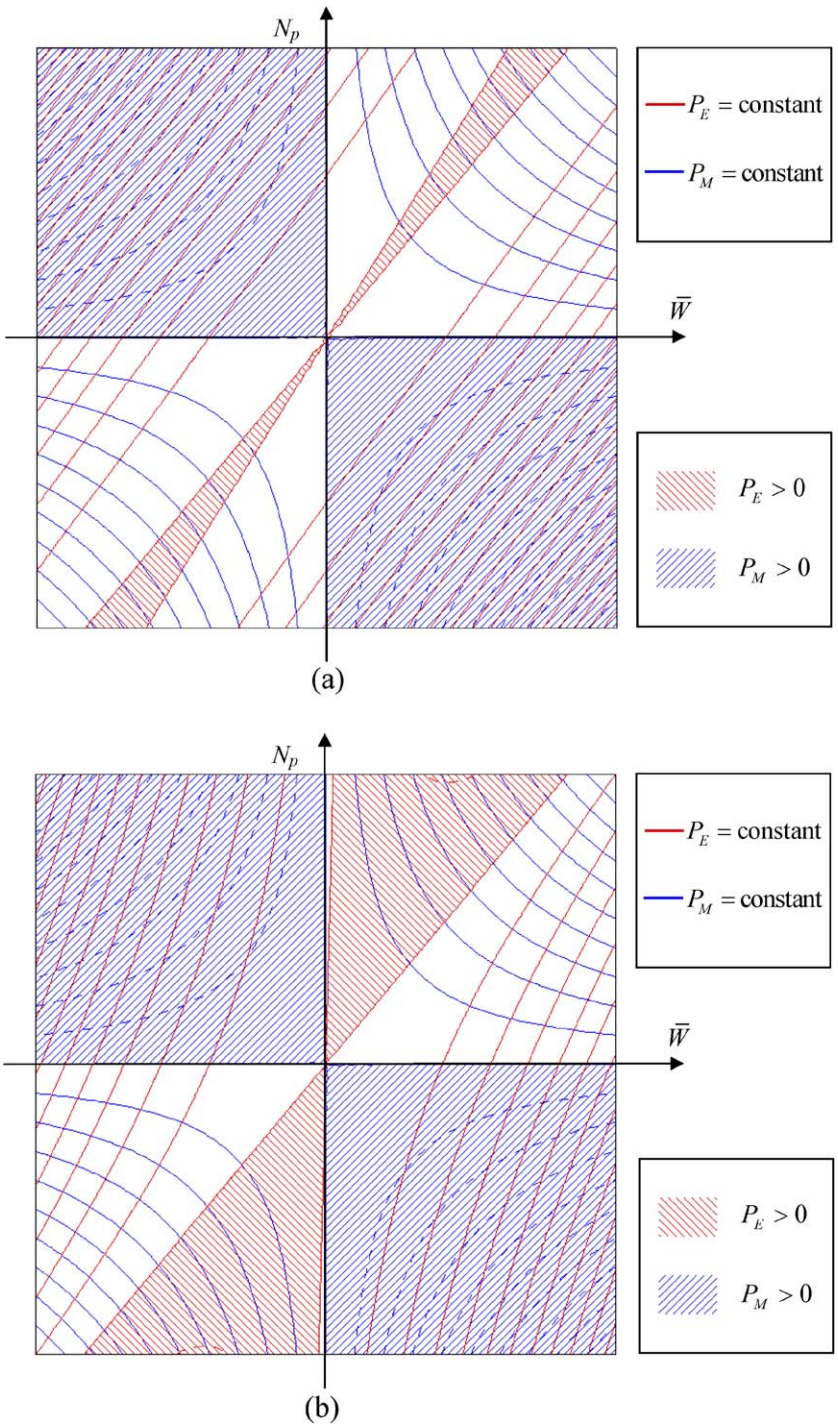

Fig. 9. Working charts in the $(\overline{W}, N_p)$ plane for a generalized MHD engine in the absence of buoyancy forces ($Gr = 0$) and for two different values of the Hartmann number M. (a) Low Hartmann number ($M = 2$); (b) high Hartmann number ($M = 1000$).

As an alternative, similar working charts can be drawn in the plane (V, N_p) or in the plane ($V, \overline{W}$). Examples can be found in Sposito and Ciofalo [14].

4.2. Working charts for the case of buoyant flow

In the presence of buoyancy forces, the average velocity is given by the more general expression (33), while the electric current is still expressed by Eq. (34) as in the no buoyancy case. The mechanical power is still expressed by Eq. (37), whereas, with respect to Eq. (38), the electric power includes now a new term depending on buoyancy:

$$P_{\mathrm{E}} = -VJ_x = -\frac{1}{M^4}\left[\left(N_p + \frac{Gr}{60}\right)^2 - (M^2+24)\left(N_p + \frac{Gr}{60}\right)\overline{W} + 12(M^2+12)\overline{W}^2\right] \tag{39}$$

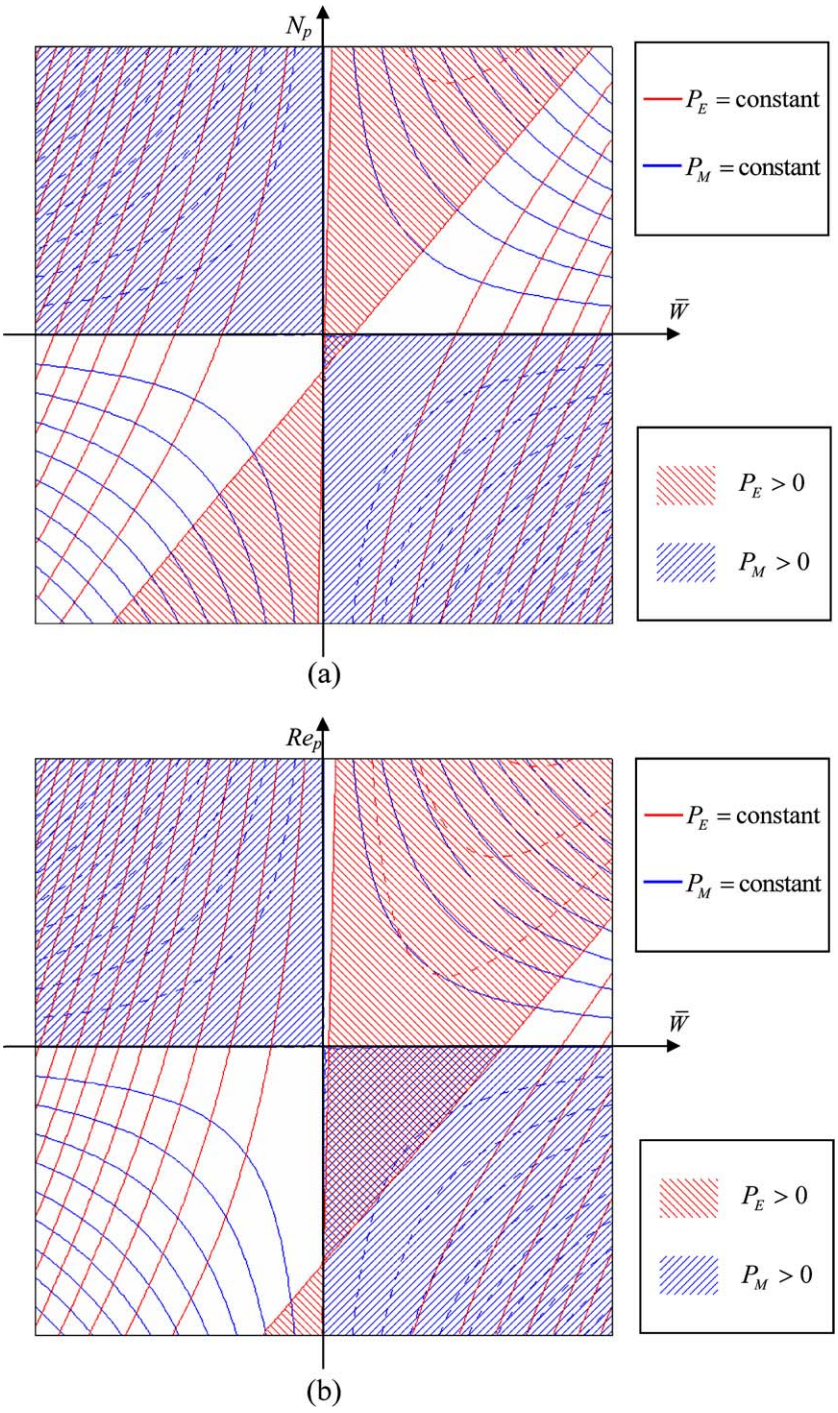

Fig. 10. Working charts in the $(\overline{W}, N_p)$ plane for a generalized MHD engine in the presence of buoyancy forces for $M = 20$ and two different values of the Grashof number Gr. (a) Low Grashof number ($Gr = 7200$); (b) high Grashof number ($Gr = 45\,000$).

The electric power P_E now vanishes for

$$N_p = 12\overline{W} - \frac{Gr}{60} \tag{40}$$

and for

$$N_p = (M^2 + 12)\overline{W} - \frac{Gr}{60} \tag{41}$$

These last two equations both represent straight lines of the $(\overline{W}, N_p)$ plane which do *not* intersect the origin of the axes. Therefore, the $(\overline{W}, N_p)$ plane is divided into 10 regions rather than 8, as shown in Fig. 10 for an intermediate value of the Hartmann number ($M = 20$) and two different values of the Grashof number Gr. It is possible to observe, for small positive values of $\overline{W}$ and negative values of N_p, a region in which the system provides *both* electric and mechanical power by converting the thermal power received, and thus operates as a (low efficiency) thermal engine.

As in the previous no-buoyancy case, working charts can also be drawn in the (V, N_p) or $(V, \overline{W})$ planes [14].

5. More general boundary conditions

The problem can be generalized by assuming the side walls to be of finite thickness and conductivity, and thus imposing the following general Cauchy conditions to the electric potential:

$$\left[\Phi + L\frac{d\Phi}{dX}\right]_{X=\pm\frac{1}{2}} = 0 \tag{42}$$

in which L is an extrapolation distance (made dimensionless by the length scale D). The solutions for W, Φ and J_x now become:

$$W(X) = \frac{1}{8}\left(\frac{Gr}{48} + N_p - \frac{M^2}{M^2+12+24L}\frac{60N_p+Gr}{60}\right) + \frac{1}{2}\left(\frac{M^2}{M^2+12+24L}\frac{60N_p+Gr}{60} - \frac{Gr}{24} - N_p\right)X^2 + \frac{Gr}{24}X^4 \tag{43}$$

$$\Phi(X) = \frac{1}{96}\left(\frac{60N_p+Gr}{5}\frac{M^2+8}{M^2+12+24L} - \frac{48N_p+Gr}{4}\right)X + \frac{1}{72}\left(-\frac{60N_p+Gr}{5}\frac{M^2}{M^2+12+24L} + \frac{24N_p+Gr}{2}\right)X^3 - \frac{Gr}{120}X^5 \tag{44}$$

$$J_x = -\frac{1}{M^2+12+24L}\frac{60N_p+Gr}{60} \tag{45}$$

while the average velocity becomes

$$\overline{W} = \frac{1}{M^2+12+24L}\frac{60N_p+Gr}{60} \tag{46}$$

For $L = 0$ the above solutions are reduced to those expressed by Eqs. (22)–(25), as obtained for the case of infinitely conducting walls. On the contrary, for $L \to \infty$ (electrically non-conducting walls), the solution becomes independent of the Hartmann number, the total electric current vanishes and all MHD effects are reduced to zero. This behaviour is observed only in one-dimensional problems, whereas in a two-dimensional channel current loops and MHD effects would exist even in the presence of insulating walls.

Another generalization of the solutions given by Eqs. (22)–(25) can be obtained by assuming the side walls to be differentially heated and/or to possess a relative velocity as in Couette flow. The corresponding boundary conditions on W and T, Eqs. (13) and (15), would change accordingly, but it can be easily shown that the solutions obtained for $\overline{W}$ and J_x, and therefore the working charts in Figs. 9 and 10, would remain unaltered.

6. Conclusions

One-dimensional analytical solutions were obtained for the steady-state, fully developed (parallel) mixed-convection flow of an electrically conducting fluid between plane parallel vertical walls under the simultaneous influence of a driving pressure head, buoyancy, and MHD forces caused by a magnetic induction field parallel to the walls. The walls were assumed to be still, isothermal, and at the same temperature, with a parabolic temperature distribution caused by a uniform internal power density; solutions were explicitly derived for different electrical boundary conditions, including equi-potential walls, an imposed electric potential drop between the walls themselves, and more general (Cauchy) conditions. The solutions could easily be generalized to take into account differentially heated and/or sliding walls.

In the case of equi-potential walls, it was found that the net electric current is proportional to the mean velocity; a particular ratio of pressure head to buoyancy forces (expressed in dimensionless terms by the condition $N_p = -Gr/60$) makes both the above quantities to vanish and cancels all MHD effects. For arbitrary values of pressure head and buoyancy, MHD effects cause the buoyancy component of the flow to decrease at most by a factor of 5, while the forced flow component decreases without limits as the Hartmann number increases. This finite reduction of the buoyant flow component is peculiar to the present one-dimensional configuration and would not be observed in two-dimensional channels having a finite extent along the direction of the magnetic field (yielding closed current loops).

In the more general case in which a difference of electric potential is imposed between the opposite walls, it is possible to define the electrical and mechanical powers P_E, P_M provided *by* the system. In a suitable state space (e.g., the plane whose axes are the dimensionless mean velocity $\overline{W}$ and pressure head N_p), according to the signs of P_E and P_M one can distinguish alternative working regimes which, in the absence of buoyancy, include direct and reverse EM pumps, direct and reverse MHD generators, and purely

dissipating modes. In the presence of buoyancy, a further regime is observed in which the system operates as a thermal engine by converting thermal power into both electrical and mechanical power.

References

[1] L. Bühler, Laminar buoyant magnetohydrodynamic flow in vertical rectangular ducts, Phys. Fluids 10 (1) (1998) 223–236.

[2] M. Ciofalo, F. Cricchio, Numerical simulation of MHD fully developed buoyant flow at low *Pr*: direct vs. "Ad Hoc" treatment of the Hartmann layers, in: Proceedings of the 19th National Conference of UIT (Unione Italiana di Termofluidodinamica), Modena, Italy, June 25–27, 2001, pp. 439–444.

[3] M. Ciofalo, F. Cricchio, Influence of a magnetic field on liquid metal free convection in an internally heated cubic enclosure, Int. J. Numer. Methods Heat Fluid Flow 12 (6) (2002) 687–715.

[4] I. Di Piazza, L. Bühler, A general computational approach for magnetohydrodynamic flows using the CFX code: buoyant flow through a vertical square channel, Fusion Technol. 38 (2) (2000) 180–189.

[5] I. Di Piazza, M. Ciofalo, Low-Prandtl number natural convection in volumetrically heated rectangular enclosures – I. Slender cavity, $AR = 4$, Int. J. Heat Mass Transfer 43 (17) (2000) 3027–3051.

[6] I. Di Piazza, M. Ciofalo, MHD free convection in a liquid-metal filled cubic enclosure – I. differential heating, Int. J. Heat Mass Transfer 45 (7) (2002) 1477–1492.

[7] I. Di Piazza, M. Ciofalo, MHD free convection in a liquid-metal filled cubic enclosure – II. Internal heating, Int. J. Heat Mass Transfer 45 (7) (2002) 1493–1511.

[8] M. Faraday, Philos. Trans R. Soc. Lond. (1832) 125–194.

[9] G.Z. Geršuni, E.M Žukovitskij, Stationary convective motions of an electrically conducting fluid between parallel planes in a magnetic field, ZETF (Zhurnal eksperimental'noi i Theoreticheskoi Fiziki) 34 (3) (1958) 670–674 (in Russian).

[10] F.A. Kulacki, D.E. Richards, Natural convection in plane layers and cavities with volumetric energy sources, in: S. Kakaç, W. Aung, R. Viskanta (Eds.), Natural Convection: Fundamentals and Applications, Hemisphere, New York, 1985.

[11] S. Mahmud, S.H. Tasnim, M.A.H. Mamun, Thermodynamic analysis of mixed convection in a channel with transverse hydromagnetic effect, Int. J. Therm. Sci. 42 (2003) 731–740.

[12] R. Moreau, Magnetohydrodynamics, Kluwer Academic Publishers, Amsterdam, 1990.

[13] E.F. Northrup, Some newly observed manifestations of forces in the interior of an electrical conductor, Phys. Rev. 24 (6) (1907) 474.

[14] G. Sposito, M. Ciofalo, Convezione Magnetoidrodinamica in Metalli Liquidi in Configurazioni Rilevanti per la Fusione Nucleare – 3. Convezione Mista in Geometrie 1-D, Quaderno N. 4/2004, Dipartimento di Ingegneria Nucleare, Università degli Studi di Palermo, 2004 (in Italian).

[15] G. Sposito, M. Ciofalo, P.A. Di Maio, G. Vella, Mixed magnetohydrodynamic convection in poloidal helium cooled lithium-lead blanket modules of a fusion reactor, in: Proceedings of the 22nd National Conference of UIT (Unione Italiana di Termofluidodinamica), Genova, Italy, 21–23 June, 2004, pp. 421–426.

[16] G. Sposito, M. Ciofalo, P.A. Di Maio, G. Vella, Mixed MHD convection and tritium transport in fusion-relevant configurations, Fusion Eng. Des. 75–79 (2005) 697–702.

[17] T. Tagawa, H. Ozoe, The natural convection of liquid metal in a cubical enclosure with various electro-conductivities of the wall under the magnetic field, Int. J. Heat Mass Transfer 41 (13) (1998) 1917–1928.